

THE DETECTION OF CRYSTALLINE SILICATES IN ULTRA-LUMINOUS INFRARED GALAXIES

H.W.W. SPOON^{1,2}, A.G.G.M. TIELENS³, L. ARMUS⁴, G.C. SLOAN¹, B. SARGENT⁵, J. CAMI⁶, V. CHARMANDARIS^{1,7,8}, J.R. HOUCK¹,
B.T. SOIFER⁴

Accepted for publication in the Astrophysical Journal, 2005 September 28

ABSTRACT

Silicates are an important component of interstellar dust and the structure of these grains – amorphous versus crystalline – is sensitive to the local physical conditions. We have studied the infrared spectra of a sample of ultra-luminous infrared galaxies. Here, we report the discovery of weak, narrow absorption features at 11, 16, 19, 23, and 28 μm , characteristic of crystalline silicates, superimposed on the broad absorption bands at 10 and 18 μm due to amorphous silicates in a subset of this sample. These features betray the presence of forsterite (Mg_2SiO_4), the magnesium-rich end member of the olivines. Previously, crystalline silicates have only been observed in circumstellar environments. The derived fraction of forsterite to amorphous silicates is typically 0.1 in these ULIRGs. This is much larger than the upper limit for this ratio in the interstellar medium of the Milky Way, 0.01. These results suggest that the timescale for injection of crystalline silicates into the ISM is short in a merger-driven starburst environment (e.g., as compared to the total time to dissipate the gas), pointing towards massive stars as a prominent source of crystalline silicates. Furthermore, amorphization due to cosmic rays, which is thought to be of prime importance for the local ISM, lags in vigorous starburst environments.

Subject headings: galaxies: ISM — ISM: evolution — infrared: galaxies — infrared: ISM

1. INTRODUCTION

Silicates are an important component of interstellar and circumstellar dust. Many Galactic sources show broad emission or absorption features at 10 and 18 μm due to the Si–O stretching and O–Si–O bending vibrations of silicate bonds. Because of the width of these features, these silicates must have an amorphous structure. These broad amorphous silicate features have also been observed in a variety of extragalactic environments, including Seyfert galaxies (e.g. Laurent et al. 2000; Clavel et al. 2000), quasars (Hao et al. 2005), luminous and ultra-luminous infrared galaxies (Genzel et al. 1998; Rigopoulou et al. 1999; Tran et al. 2001; Spoon et al. 2004; Armus et al. 2004) and a sample of mid-infrared detected, optically invisible, high-luminosity galaxies with redshifts of $1.7 < z < 2.8$ (Houck et al. 2005).

In recent years, observational evidence for the presence of *crystalline* silicates in various astrophysical environments has also emerged. In particular, infrared spectra have revealed that silicates in circumstellar environments often contain a significant crystalline fraction around both pre-main-sequence stars (T-Tauri stars and Herbig AeBe stars) and post-main-sequence stars (Asymptotic Giant Branch (AGB) stars, post-AGB stars, planetary nebulae, Luminous Blue Variables (LBVs), Red Super Giants (RSGs) and post-RSGs) (e.g. Acke et al. 2004; Malfait et al. 1998; Molster et al. 2002; Sylvester et al. 1999; van Boekel et al. 2004; Voors et al. 1999, 2000). These crystalline silicates are invariably magnesium rich (e.g., pyroxene (MgSiO_3) and

forsterite (Mg_2SiO_4). Crystalline silicates are also known to be ubiquitous in the solar system, including primitive objects such as comets (e.g. Crovisier et al. 1997; Hanner et al. 1999; Wooden et al. 1993). Because crystallization is inhibited by high-energy barriers, the origin and evolution of the crystalline silicate fraction in interstellar and circumstellar media has the potential to provide direct evidence of energetic processing of grains.

Silicates play an especially large role in shaping the mid-infrared spectral appearance of Ultra-Luminous InfraRed Galaxies (ULIRGs; $L_{\text{IR}} \geq 10^{12} L_{\odot}$). ULIRGs are thought to represent the final stage in the merging process of gas-rich spirals, where the interaction has driven gas and dust towards the remnant nucleus, fueling a massive starburst and a nascent active galactic nucleus (AGN). Here, we present evidence for the presence of *crystalline* silicates as part of the deep silicate absorption features observed towards a sample of twelve heavily obscured ULIRGs.

2. OBSERVATIONS AND DATA REDUCTION

We are obtaining mid-infrared spectroscopy for a sample of 110 ULIRGs, as part of the Guaranteed Time Observation (GTO) ULIRG program of the Infrared Spectrograph (IRS)⁹ (Houck et al. 2004) on the Spitzer Space Telescope (Werner et al. 2004). Seventy seven of these spectra have been analyzed so far.

The twelve ULIRG spectra presented in this paper were selected based upon the strength of spectral structure indicative of crystalline silicate absorption bands at 16 and 23 μm . Table 1 lists the basic properties of these targets, along with their observation dates and on-source integration times.

The observations were made with the Short-Low (SL) and Long-Low (LL) modules of the IRS. The spectra were extracted from the flatfielded images provided by the Spitzer Science Center (pipeline version S11.0.2). The images were background-subtracted by differencing the two SL apertures

¹ Cornell University, Astronomy Department, Ithaca, NY 14853

² Spitzer fellow

³ SRON National Institute for Space Research and Kapteyn Institute, P.O. Box 800, 9700 AV Groningen, The Netherlands

⁴ Caltech, Spitzer Science Center, MS 220-6, Pasadena, CA 91125

⁵ University of Rochester, Department of Physics and Astronomy, Rochester, NY 14627

⁶ NASA-Ames Research Center, MS 245-6, Moffett Field, CA 94035

⁷ Department of Physics, University of Crete, GR-71003, Heraklion, Greece

⁸ Chercheur Associé, Observatoire de Paris, F-75014, Paris, France

⁹ The IRS was a collaborative venture between Cornell University and Ball Aerospace Corporation funded by NASA through the Jet Propulsion Laboratory and the Ames Research Center

TABLE 1
PROPERTIES OF SOURCES

Target	AOR key	Date observed	Int. time min.	redshift	D_L Mpc ^a
00183-7111	7556352	14 Nov. 2003	15	0.327	1700
00397-1312	4963584	04 Jan. 2004	14	0.262	1320
01199-2307	4964864	18 Jul. 2004	14	0.156	737
06301-7934	4970240	11 Aug. 2004	12	0.156	700
06361-6217	4970496	11 Aug. 2004	14	0.160	760
08572+3915	4972032	15 Apr. 2004	6	0.0584	258
15250+3609	4983040	4 Mar. 2004	7	0.0554	244
Arp220	4983808	29 Feb. 2004	5	0.0181	78
17068+4027	4986112	16 Apr. 2004	14	0.179	858
18443+7433	4987904	5 Mar. 2004	14	0.135	627
20551-4250	4990208	14 May 2004	4	0.0427	186
23129+2548	4991488	17 Dec. 2003	23	0.179	858

^aassuming $H_0=71 \text{ km s}^{-1} \text{ Mpc}^{-1}$, $\Omega_M=0.27$, $\Omega_\Lambda=0.73$, $\Omega_K=0$

and for LL, by differencing the two nod positions. Spectra were then extracted and calibrated using the *IRS* standard star HR 6348 for SL and the stars HR 6348, HD 166780, and HD 173511 for LL (Sloan et al. 2005). Small wavelength corrections were made to compensate for known offsets in the S11 processed data. After extraction the orders were stitched to LL order 1, requiring order-to-order scaling adjustments of typically 5–10%. The largest adjustment was made for Arp 220 to match SL order 1 and LL order 2, which required SL1 to be scaled up by 21%. In the final step, the 5–37 μm spectra were scaled to match the observed *IRS* blue or red peak-up flux. For those sources lacking a (useful) peak-up flux, the spectra were scaled down by 10%, the average scaling factor of the other spectra. In some spectra, most notably in IRAS 20551–4250, residual fringing, which is due to sub-pixel pointing errors, appears in LL order 1 (between 20 and 30 μm).

3. ANALYSIS

The top panel of Figure 1 shows the average *IRS* low-resolution spectrum for our sample, obtained after scaling the spectra to $S_\nu = 1 \text{ Jy}$ at 15 μm . The average spectrum is dominated by broad absorption features at 10 and 18 μm , which we attribute to absorption by amorphous silicates. The spectrum further shows weaker absorption features due to water ice (6.0 μm) and hydrocarbons (6.90 and 7.25 μm). PAH emission features can be seen at low contrast at 6.2, 7.7, and 11.2 μm . The features are especially weak in the spectrum of IRAS F00183–7111 (Spoon et al. 2004) and absent in the spectrum of IRAS 08572+3915 (Figure 1, lower panel). Our spectra further show a few emission lines, most notably the $\text{H}_2 \text{S}(3)$ line at 9.66 μm , the $[\text{NeII}]$ line at 12.81 μm and the $\text{H}_2 \text{S}(1)$ line at 17.0 μm . These will be discussed elsewhere (Armus et al. 2005; Higdon et al. 2005).

Upon close inspection, the spectra also reveal evidence for weak and narrow absorption features near 16, 19 and 23 μm , independent of the redshift of the source. Emission and absorption features at these wavelengths are also known in Galactic sources with strong silicate features and have been attributed to the presence of crystalline silicates.

In order to investigate the presence of a crystalline component to the silicate absorption features in our sample, we infer the silicate optical depth spectrum by dividing out a local continuum from our *IRS* spectra. We define the local continuum as a three point spline interpolation of continuum points at 5.6 μm (0.1 μm shortward of the wavelength range affected by the 6.0 μm water ice absorption feature),

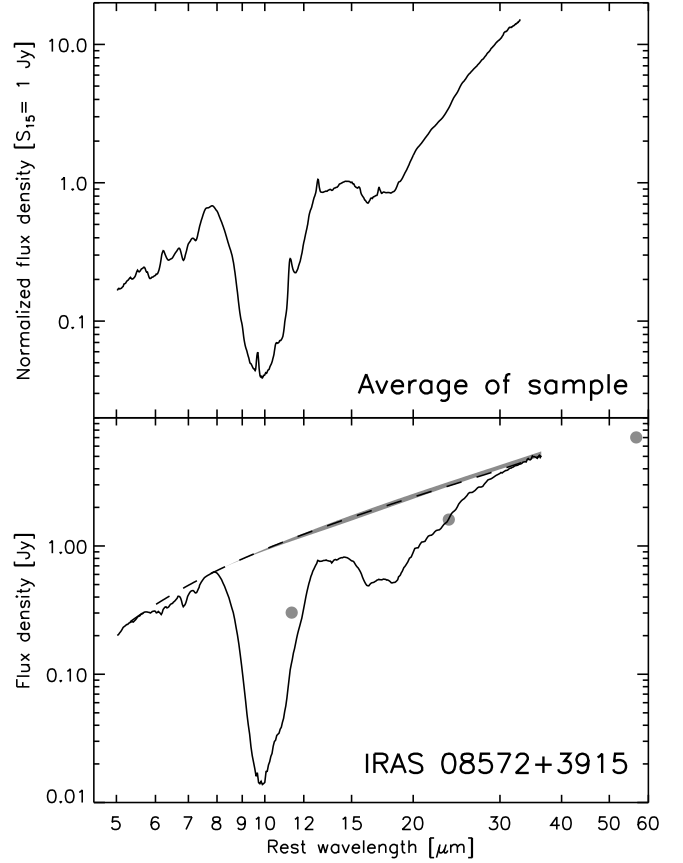


FIG. 1.— Upper panel: the average 5–32 μm spectrum of the 12 ULIRGs in our sample after normalizing each spectrum individually at 15 μm . Features and lines are identified in the text. Lower panel: the 5–60 μm spectrum of IRAS 08572+3915. The *IRS* low-resolution spectrum (black) is shown together with the 12, 25 and 60 μm *IRAS* fluxes (grey filled circles). Three choices for the local continuum are indicated by the black dashed line and grey shaded area. Error bars are omitted in both panels, because of the high S/N of the data

7.1 μm (in between the two hydrocarbon absorption bands at 6.90 and 7.25 μm), and the red cut-off of *IRS* LL order 1 (ranging from 29 to 36 μm , depending on the redshift of the source). For sources without discernable 7.7 μm PAH emission (e.g. IRAS 08572+3915 and IRAS F00183–7111), we replace the 7.1 μm pivot by the continuum at 7.9–8.0 μm . The resulting spline interpolated local continuum is illustrated for IRAS 08572+3915 in the lower panel of Figure 1. The effect of small changes in the adopted local continuum on the resulting silicate profile is illustrated by the shaded areas around the spline-interpolated continuum in the lower panel of Figure 1 and on the resulting silicate profile in the third panel of Figure 2. The resulting optical depth profiles for the twelve sources in our sample have apparent 10 μm optical depths ranging from 2.1 for IRAS 17068+4027 to 4.2 for IRAS 08572+3915, with a mean value of 2.5 (see Figure 3 and Table 2).

In order to derive the characteristics of these narrow features we have to account for the amorphous silicate features which dominate the absorption structure in this wavelength range. We have compared the general profile of the 10 and 18 μm amorphous silicate features in these ULIRGs with those in a sample of Galactic background sources (Chiar & Tielens 2005). However, because of the uncertainties in the placement of the continuum for these Galactic sources, the derived inter-

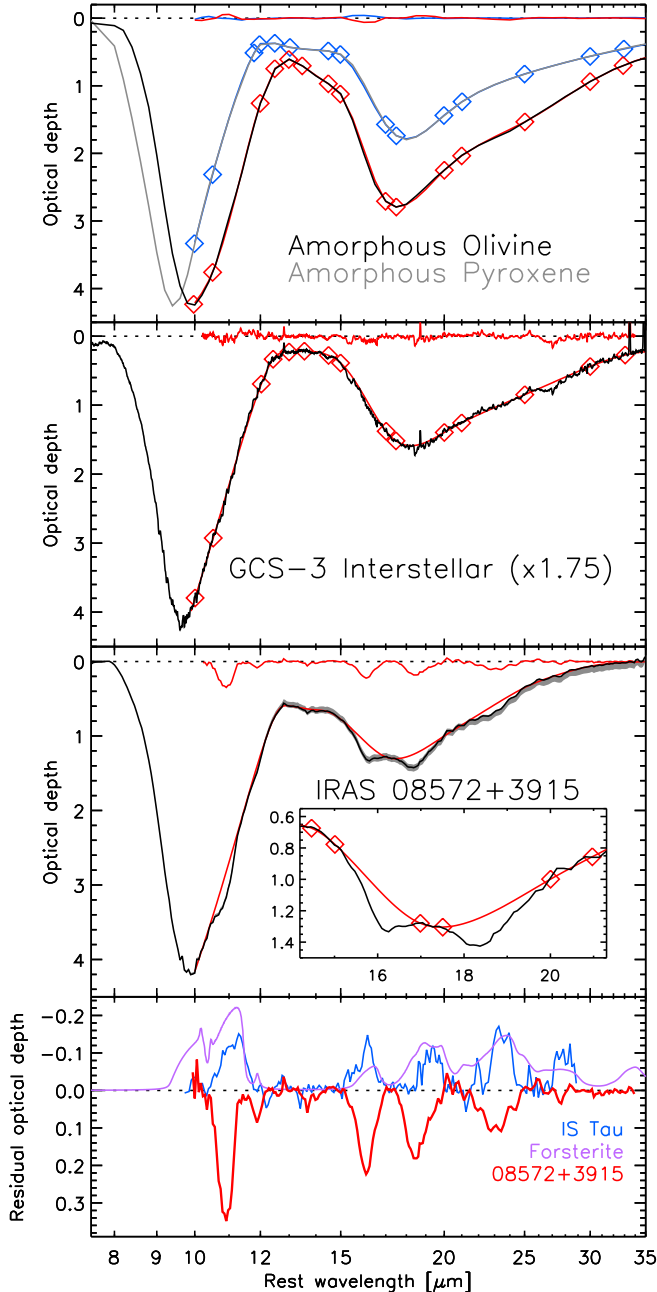


FIG. 2.— Illustration of our method for fitting the amorphous component of silicate absorption features. Upper panel: laboratory opacity spectra of amorphous olivine (black) and amorphous pyroxene (grey), presented as optical depth profiles. Overlaid are spline fits (red, blue), presented as optical depth profiles. Overlaid are spline fits (red, blue) to pre-selected wavelength pivots (red, blue diamonds). Fit residuals, indicating imperfections in the fitting method, are shown as deviations from zero optical depth (red, blue). Second panel: spline fit (red) to the GCS 3 optical depth profile (black; scaled-up by a factor 1.75). Fit residuals are shown as deviations from zero optical depth (red). Third panel: the optical depth spectrum of IRAS 08572+3915 (black). The grey shading indicates the effect of a different choice of local continuum on the resulting optical depth profile; see Figure 1. The red curve is a spline fit to the amorphous silicate profile, ignoring the narrow substructure near 11, 16, 19 and 23 μm . The residual spectral structure, shown in red at the top of this panel, is too strong to be attributed to imperfections in the fitting method. Instead we attribute the features at 11, 16, 19 and 23 μm to crystalline silicates. Third panel inset: a close-up of the 14–21 μm range, demonstrating the prescribed placement of spline pivots at 14.5, 15.0, 17.0, 17.5, 20.0 and 21.0 μm . Lower panel: the residual optical depth spectrum of IRAS 08572+3915 (red) is compared to the residual crystalline silicate emissivity of the disk around the young star IS Tau (blue) and the opacity profile of forsterite (purple). Both have been scaled by arbitrary factors.

stellar 10 and 18 μm amorphous silicate features show differences in their relative strengths, and in the level of absorption between them. Since fitting the ULIRG data with a composite Galactic spectrum would therefore introduce spurious artifacts, we have elected to represent the broad amorphous silicate features in the ULIRG and Galactic spectra with spline fits. Deviations from these fits in the ULIRG spectra, significantly larger than those seen among the Galactic sources, would then argue strongly for a crystalline component. We have tested this procedure on the high signal-to-noise spectrum of the Galactic Center Source GCS 3, and on laboratory absorption spectra of amorphous silicates. The residuals from the spline fits to these spectra are very small ($<6\%$), validating our analysis to that level.

The method is demonstrated in the top panel of Figure 2 for laboratory spectra of amorphous olivines and pyroxenes (Fabian et al. 2001). The spline fit traces the amorphous profile to better than 2% of the local optical depth, except for the 16 μm range, where the spline deviates by up to 6%. The resulting small artifacts are shown at the top of the panel. We also tested our method on the optical depth profile as seen towards the Galactic background source GCS 3 (Chiar & Tielens 2005), depicted in the second panel of Figure 2. The silicates along this line of sight are thought to be $>99\%$ amorphous in composition (Kemper et al. 2004, 2005). In contrast to the laboratory profiles, the fit residuals for the GCS 3 spectrum are dominated by spectral noise rather than fitting artifacts. The third panel of Figure 2 shows the fit to the silicate profile of the ULIRG IRAS 08572+3915. The red curve smoothly fits the maximum depth of the broad 18 μm feature, while ignoring the strong, narrow substructure around 11, 16, 19 and 23 μm . After subtracting the spline-interpolated amorphous component from the optical depth spectrum, the features at 11, 16, 19 and 23 μm show up in the fit residual spectrum, clearly above the levels expected for artifacts introduced by the fitting procedure. In the lower panel of Figure 2 we compare these residuals to known spectra of circumstellar and laboratory crystalline silicates.

The adopted spline fits to the amorphous silicate profiles for the twelve ULIRGs in our sample are overplotted in red in Figure 3, while the residual optical depth spectra are presented in Figure 4. The individual spectra in the latter figure are truncated at -0.1 optical depth in order not to be dominated by spurious optical depth structure introduced by emission features of 11.3 μm PAH and 12.8 μm [Ne II]. These common features aside, the twelve spectra clearly show absorption structure at 16, 19 and 23 μm that cannot be attributed to observational artifacts (i.e. fringing, flux calibration) or imperfections in the spline fit to the amorphous component. A few sources (e.g. IRAS 06301–7934, IRAS 23129+2548) further show a weak feature at 27–28 μm and only one source, IRAS 08572+3915, a strong feature at 11 μm (see also Figure 2). The latter feature may also be present in the other spectra, but its detection is complicated by the presence of emission from 10.51 μm [S IV] and 11.3 μm PAH in the same wavelength range (see Figure 4). Further note the presence of absorption bands of gas phase C_2H_2 and HCN at 13.7 and 14.05 μm in the spectra of several of our ULIRGs, most notably IRAS 15250+3609 and IRAS 23129+2548. These bands are otherwise seen in dense, warm molecular clouds surrounding massive Galactic proto-stars (Lahuis & van Dishoeck 2000).

In Figure 5 we show the average residual optical depth spectrum for our twelve sources and compare it to the observed crystalline silicate opacity profile of the young star IS

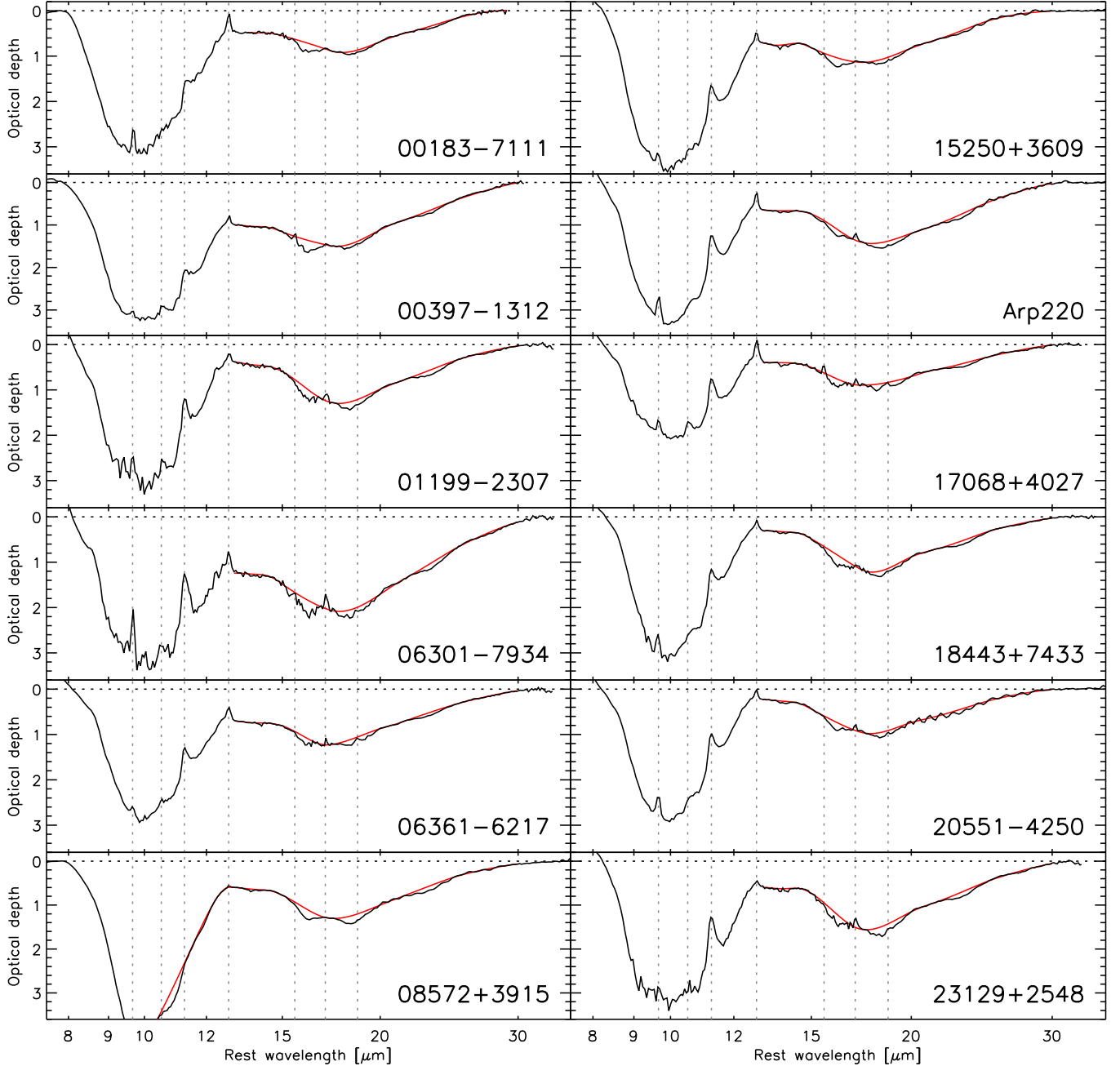


FIG. 3.— 8–30 μm optical depth spectra for the 12 ULIRGs in our sample. The *red* curve is a spline fit to the amorphous silicate profile, ignoring the narrow substructure at 11, 16, 19, 23 and 28 μm . Vertical dotted lines indicate the positions of 9.66 μm $\text{H}_2\text{S}(3)$, 10.5 μm $[\text{SiV}]$, 11.3 μm PAH, 12.8 μm $[\text{NeII}]$, 15.5 μm $[\text{NeIII}]$, 17.0 μm $\text{H}_2\text{S}(1)$ and 18.7 μm $[\text{SiII}]$.

Tau (Sargent et al. 2005) and the calculated opacity profile of forsterite (Fabian et al. 2001). The relative strengths of the absorption bands in the ULIRG spectra are different from those of the comparison profiles. In the ULIRG spectra, the features get progressively weaker towards longer wavelength, whereas no such trend exists for the comparison profiles (see also Figures 2 and 5). A possible explanation for this trend could be dilution of the crystalline absorption spectrum by cold dust emission from a less obscured cooler component, either the other nucleus or the circumnuclear environment. Nevertheless, the similarities between the ULIRG profile and the comparison profiles in peak position and width are striking. We therefore conclude that the features observed at 11, 16, 19,

23 and 28 μm in the ULIRG spectra are indeed caused by the presence of crystalline silicates in their nuclear medium.

The peak position of the 16 μm band, in particular, is sensitive to the Mg/Fe ratio of olivines (Koike et al. 2003). The peak position of this band observed in the ULIRG spectra (16.1 μm) falls close to the laboratory measured position of forsterite, the Mg-rich end member of the olivines (Mg_2SiO_4 ; 16.3 μm ; Koike et al. 2003) and much to the blue of the peak position in fayalite, the iron-rich end member of the olivines (Fe_2SiO_4 ; 17.7 μm ; Koike et al. 2003). Hence, in line with other observations of crystalline silicates in space, extragalactic olivines appear to be extremely Mg-rich and Fe-poor.

We infer the fraction of crystalline silicates in our sample

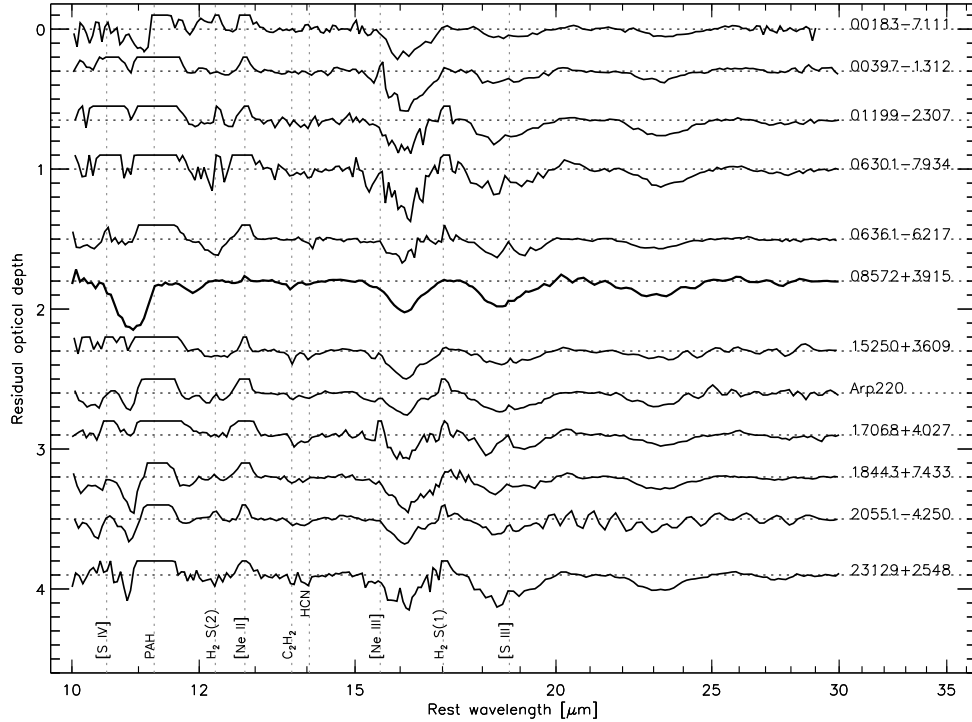


FIG. 4.— 10–30 μm residual optical depth spectra for the 12 ULIRGs in our sample after subtraction of the amorphous silicate component from the optical depth spectra. For plotting purposes, the spectra have been offset and truncated at residual optical depths of -0.1. Crystalline silicate features can be identified at 11, 16, 19, 23 and 28 μm

TABLE 2
AMORPHOUS AND CRYSTALLINE SILICATES

Target	$\tau_{am}(\text{peak})^a$	$\tau_{cr}(\text{peak})^b$	$\tau_{cr}(\text{peak})/\tau_{am}(\text{peak})$	N_{cr}/N_{am}^c
00183–7111	3.0	0.22	0.073	0.11
00397–1312	3.2	0.28	0.088	0.13
01199–2307	3.6	0.21	0.060	0.09
06301–7934	3.4	0.35	0.10	0.15
06361–6217	2.9	0.15	0.051	0.08
08572+3915	4.2	0.22	0.053	0.08
15250+3609	3.6	0.20	0.056	0.08
Arp220	3.3	0.16	0.048	0.07
17068+4027	2.1	0.17	0.082	0.12
18443+7433	3.2	0.25	0.078	0.12
20551–4250	2.9	0.18	0.062	0.09
23129+2548	3.2	0.25	0.078	0.12

^aapparent peak optical depth of the 10 μm feature

^bapparent peak residual optical depth of the 16 μm feature

^cassuming $N_{cr}/N_{am} = 1.5 \times \tau_{cr}(\text{peak})/\tau_{am}(\text{peak})$; see eq. (1)

from the peak optical depths of the 10 μm amorphous and the 16 μm crystalline silicate absorption bands using

$$\frac{N_{cr}}{N_{am}} = \frac{\tau_{cr}(\text{peak})}{\tau_{am}(\text{peak})} \times \frac{\kappa_{am}(\text{peak})}{\kappa_{cr}(\text{peak})} \quad (1)$$

where N_{am} and N_{cr} are the mass column densities of the amorphous and crystalline silicates. Adopting $\kappa_{am}(\text{peak}) = 2.4 \times 10^3 \text{ cm}^2/\text{g}$ as the peak mass absorption coefficient for amorphous silicates (Dorschner et al. 1995) and $\kappa_{cr}(\text{peak}) = 1.6 \times 10^3 \text{ cm}^2/\text{g}$ as the peak mass absorption coefficient for forsterite (Fabian et al. 2001), we find crystalline-to-amorphous silicate mass column density ratios ranging from 0.07 to 0.15, with a median value of 0.11 (see Table 2). It should be understood that these numbers are upper limits, since foreground emission and radiative transfer effects within the optically thick 10 μm silicate band may cause the apparent

optical depth of the 10 μm silicate feature to be a lower limit to the true optical depth. Our findings should be contrasted to the upper limit of crystalline silicates in the general ISM of the Milky Way of $<1\%$ (Kemper et al. 2004, 2005) and the crystalline-to-amorphous ratios of up to 0.75 observed in circumstellar environments (Molster et al. 2002).

Given the broad range in inferred crystalline-to-amorphous silicate ratios in our sample, we have investigated the existence of correlations with the apparent 10 μm optical depth, the IRAS R(60,100) color, the 5.5 μm -to-23 μm rest frame spectral slope and the 6.2 μm PAH equivalent width, but found no significant trends. The fraction of crystallinity within this sample can therefore, at present, not be linked to the infrared spectral appearance.

4. DISCUSSION

We have detected crystalline substructure in the silicate absorption features towards twelve strongly obscured ULIRG nuclei. This is the first detection of crystalline silicates in any source outside the Local Group. Space-based and ground-based observations have revealed the presence of infrared emission features of crystalline silicates around young stellar objects and evolved stars (Acke et al. 2004; Malfait et al. 1998; Molster et al. 2002; Sylvester et al. 1999; van Boekel et al. 2004; Voors et al. 1999, 2000). Comets also often show evidence for crystalline silicates in their spectra (Crovisier et al. 1997; Hanner et al. 1999; Wooden et al. 1993). In contrast, while stellar sources of silicate dust inject at least 5% of their silicates in crystalline form, the Galactic *interstellar* silicate feature is exceedingly smooth, and there is no evidence for a crystalline absorption component in the Galactic ISM. This translates into an upper limit on the crystalline fraction in the Galactic interstellar medium of 1% (Kemper et al. 2004, 2005). This difference in crystallinity

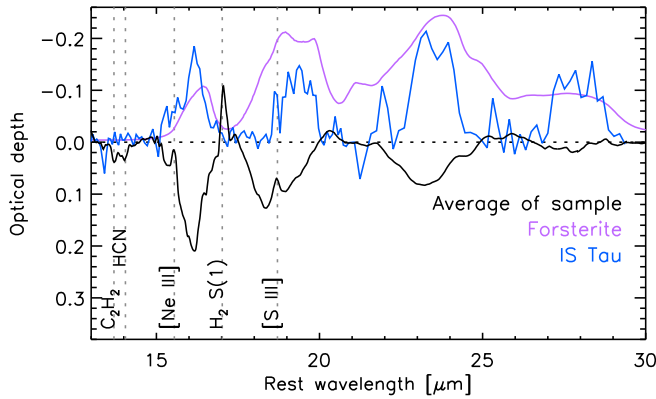


FIG. 5.— The average 13–30 μm residual optical depth spectrum for our sample (black) compared to the residual crystalline silicate emissivity of the disk around the young star IS Tau (blue) and the opacity profile of forsterite (purple). Both have been scaled by arbitrary factors

between silicates injected and silicates in the ISM implies a rapid transformation of crystalline silicates into amorphous silicates in the interstellar medium ($\lesssim 10^8$ yr; Kemper et al. 2004, 2005). This transformation has been attributed to energetic processing of the dust by heavy cosmic ray ions (Bringa et al. 2005) or to ion bombardment in high velocity ($v > 1000$ km/s) shocks (Jäger et al. 2003; Rotundi et al. 2002; Demyk et al. 2004). In particular, based upon laboratory experiments and estimated cosmic ray fluxes in our galaxy, the timescale for amorphization is estimated to be only 70 million years (Bringa et al. 2005), considerably shorter than the timescale at which (crystalline) silicates are injected into the Galactic ISM (4 billion years; Bringa et al. 2005).

These same processes — injection of crystalline silicates from stars and cosmic ray and shock amorphization — will play a role in the interstellar media of these ULIRGs as well. Possible explanations for the much higher crystalline silicate fraction in these ULIRGs as compared to the Milky Way include a higher fraction of crystalline silicates injected and/or a delay in the interstellar amorphization rate.

In particular, ULIRGs are characterized by a high rate of star formation driven by merging events. In contrast to the local ISM, the enrichment of the dusty interstellar medium will be dominated by the rapidly evolving massive stars and the contribution by the more numerous low-mass stars will lag on the timescale associated with the ULIRG-merger event (10^8 – 10^9 yr; Murphy et al. 1996, 2001). Evidence for the presence of a large population of evolved massive stars in ULIRG nuclei exists for the nearest ULIRG, Arp 220 (Armus et al. 1995). Spectroscopic studies of sources in our galaxy have revealed that massive stars are prominent sources of crystalline silicates during the supergiant phase. In particular, the more extreme examples of this class, such as AFGL 4106, NML Cyg and IRC +10420, have crystalline silicate fractions of the order of 0.15 (Molster et al. 1999). Likewise, crystalline silicates have been observed in the ejecta of some LBVs, such as R 71 and AG Car (Voors et al. 1999, 2000). This episodic mass-loss phase dominates the dust injection by the most massive stars ($M > 50 M_{\odot}$) in the Galaxy. Finally, it is currently unknown how much crystalline silicate dust is injected by supernovae. Indeed it is unknown how much dust is injected by SNe. However, it is conceivable that the SNe resulting from this starburst also inject a large fraction of their freshly condensed dust in the form of crystalline silicates. Hence, a starburst may rapidly increase the crystalline

silicate fraction in the nuclear region.

Of course, the high supernova rate in a starburst will drive strong shock waves into the local environment, which will sputter the dust, returning the atoms from the solid to the gas phase (Jones et al. 1994, 1996). However, likely, the destruction rate of crystalline and amorphous silicates are similar and hence, to first order, this will not affect the crystalline-to-amorphous fraction. More importantly, supernovae are thought to be the dominant source of cosmic rays and this may increase the rate at which crystalline silicates are transformed into amorphous silicates. However, cosmic rays freshly accelerated in the supernova remnants may leak away to the rest of the galaxy on a timescale of $\sim 10^6$ yr (Webber 1993), limiting the rate of this solid-state conversion in the starburst environment. Thus, the crystalline-to-amorphous conversion timescale may actually be quite similar to the value calculated for the local Milky Way (70 million years; Bringa et al. 2005). We expect that over time, as the merging event ages and the starburst intensity decreases, the fraction of crystalline silicates will decrease on a similar time-scale. Thus, we attribute the high fraction of crystalline silicates in these ULIRGs as compared to others to the relative ‘youth’ of these systems; e.g., the amorphization process may lag the merger-triggered, star-formation-driven dust injection process.

All 17 ULIRGs with $\tau(10 \mu\text{m}) > 2.9$ in our ULIRG sample of 77 galaxies show crystalline silicate structure in their IRS spectra. At lower silicate optical depth, the number of clear detections falls sharply. Above $\tau(10 \mu\text{m}) = 2$, 18 out of 23 ULIRGs definitely show the 16 μm crystalline feature. Above $\tau(10 \mu\text{m}) = 1$, this is 20 out of 46 and for the entire ULIRG sample only 21 out of 77. We note that a complete analysis of this fraction is hampered by possible radiative transfer effects in the silicate features (as evidenced by the strong variation in the ratio of 10–to–18 μm peak optical depths), the presence of 16–18 μm UIR emission in some sources with non-negligible PAH emission (Brandl et al. 2005) and by the challenge to detect weak 16 μm absorption features at low contrast and low signal-to-noise. Nevertheless, it is clear that crystalline silicates are a common component of the nuclear interstellar medium during the strongly obscured evolutionary phase of the ULIRG phenomena.

Crystalline silicates can also be a sign of high-temperature grain processing. In a ULIRG, both a central AGN and hot, young stars are potential sources of high-energy photons capable of heating the dust in the ISM. X-ray and far UV photons from a central AGN will produce a hot, inner region. However, an AGN as the source of grain processing in our ULIRG sample is problematic for two reasons. First, interferometric 10 μm spectra of the Seyfert-2 nucleus of NGC 1068 do not show any indication for crystalline silicates in its inner warm 2 pc region (Jaffe et al. 2004). Second, the crystalline silicates are seen in absorption in our spectra, implying that they are located in the cooler, outer regions. This would require a large scale mechanism to transport the inner toroid material outwards and distribute it over the surrounding medium. The extended nature of a starburst does not require such a mechanism and therefore seems a more likely source of processed material than a central source.

Crystalline silicates are also a characteristic of the circumstellar planetary disks surrounding young stellar objects such as Herbig AeBe stars and T-Tauri stars. Again, in order to be seen in absorption, this material will have to be transported outwards into the surrounding cold medium, presumably through jets and winds (Tielens 2003). There is,

however, no indication in Galactic sources for such large scale transport of crystalline silicates. On the contrary, for Herbig AeBe stars the emission features of crystalline silicates are strongly concentrated towards the inner 2 AU of the disks (e.g., van Boekel et al. 2004). Hence, we deem high-temperature crystallization of existing amorphous silicate grains unlikely as the source of the high crystalline silicate fraction in ULIRGs.

5. CONCLUSIONS

In this work, we report the discovery of crystalline substructure at 11, 16, 19, 23 and 28 μm in the amorphous silicate features towards twelve deeply obscured ULIRG nuclei. These features indicate the presence of the mineral forsterite (Mg_2SiO_4). Previously, crystalline silicates have only been observed in circumstellar environments.

We infer the fraction of crystalline silicates in our sample from the peak optical depths of the 10 μm amorphous and the 16 μm crystalline bands and find a crystalline-to-amorphous ratio ranging from 0.07 to 0.15, with a median value of 0.11. These numbers are likely upper limits, since foreground emission and radiative transfer effects will cause the apparent 10 μm silicate optical depth to be a lower limit to the true optical depth.

The crystalline-to-amorphous ratio in our twelve deeply obscured ULIRGs is 7–15 times larger than the upper limit for this ratio in the interstellar medium of the Milky Way. This suggests that the timescale for injection of crystalline silicates into the ISM is short in a merger-driven starburst environment

(e.g., as compared to the total time to dissipate the gas), pointing towards evolved massive stars (red supergiants, LBVs and type II supernovae) as prominent sources of crystalline silicates. Furthermore, the timescale for amorphitization of crystalline silicates, which is known to be fairly rapid in the ISM of the Milky Way ($\sim 10^8$ yr), is at most of similar order in starburst environments. We expect that over time, as the merging event ages and the starburst decreases in intensity, the fraction of crystalline silicates will decrease rapidly. Thus, we attribute the high fraction of crystalline silicates in these ULIRGs, as compared to others, to the relative ‘youth’ of these systems.

Finally, other galaxy types may also exhibit crystalline silicate features far above the upper limits set for the crystalline silicate fraction in the ISM of our galaxy ($< 1\%$; Kemper et al. 2004, 2005). The possible detection of a 23 μm crystalline emission feature in the quasar PG 1351+640, reported by Hao et al. (2005), may be a signpost of more detections to come.

The authors wish to thank Elise Furlan, Bill Forrest, Patrick Morris, Els Peeters for discussions, and Frank Molster and Sacha Hony for sharing their ISO–SWS data. Support for this work was provided by NASA through Contract Number 1257184 issued by the Jet Propulsion Laboratory, California Institute of Technology under NASA contract 1407. HWWs was supported under this contract through the Spitzer Space Telescope Fellowship Program.

REFERENCES

- Acke, B., van den Ancker, M.E., 2004, *A&A*, 426, 151
 Armus, L., Neugebauer, G., Soifer, B.T., Matthews K., 1995, *AJ*, 110, 2610
 Armus, L., et al., 2004, *ApJS*, 154, 178
 Armus, L., et al., 2005, in preparation
 Brandl, B.R., et al., 2005, in preparation
 Bringa, E.M., et al., 2005, submitted
 Chiar, J.E., Tielens, A.G.G.M., 2005, in preparation
 Clavel, J., Schulz, B., Altieri, B., Barr, P., Claes, P., Heras, A., Leech, K., Metcalfe, L., Salama, A., 2000, *A&A*, 357, 839
 Crovisier, J., et al., 1997, *Science*, 275, 1904
 Demyk K., d’Hendecourt, L., Keroux, H., Jones, A.P., Borg, J., 2004, *A&A*, 420, 547
 Dorschner, J., Begemann, B., Henning, T., Jäger, C., Mutschke, H., 1995, *A&A*, 300, 503
 Fabian, D., Henning, T., Jäger, C., Mutschke, H., Dorschner, J., Wehrhan, O., 2001, *A&A*, 378, 228
 Gail, H.P., 2004, *A&A*, 413, 571
 Genzel R., et al., 1998, *ApJ* 498, 579
 Hannner, M., 1999, *Space Sci Rev*, 90, 99
 Hao, L., et al., 2005, *ApJ*, 625, 75
 Higdon, S.J.U., et al., 2005, in preparation
 Houck, J.R., et al. 2004, *ApJS*, 154, 18
 Houck, J. R., et al. 2005, *ApJ*, 622, L105
 Jaffe, W., et al. 2004, *Nature*, 429, 47
 Jäger C., et al., 2003, *A&A*, 401, 57
 Jones, A.P., Tielens, A.G.G.M., Hollenbach, D.J., McKee, C.F., 1994, *ApJ*, 433, 797
 Jones, A.P., Tielens, A.G.G.M., Hollenbach, D.J., 1996, *ApJ*, 469, 740
 Kemper, F., Vriend, W.J., Tielens, A.G.G.M., 2004, *ApJ*, 609, 826
 Kemper, F., Vriend, W.J., Tielens, A.G.G.M., 2005, erratum
 Koike, C., Chihara, H., Tsuchiyama, A., Suto, H., Sogawa, H., Okuda, H., 2003, *A&A*, 399, 1101
 Lahuis, F., van Dishoeck, E.F., 2000, *A&A*, 355, 699
 Laurent, O., Mirabel, I.F., Charmandaris, V., Gallais, P., Madden, S.C., Sauvage, M., Vigroux, L., Cesarsky, C., *A&A*, 359, 887
 Leitherer, C., et al., 1999, *ApJS*, 123, 3
 Malfait, K., et al., 1998, *A&A*, 332, L25
 Molster, F., et al., 1999, *A&A* 350, 163
 Molster, F., Waters, L.B.F.M., Tielens, A.G.G.M., Koike, C., Chihara, H., 2002, *A&A*, 382, 241
 Murphy, T.W., Armus, L., Matthews, K., Soifer, B.T., Mazzarella, J.M., Shupe, D.L., Strauss, M.A., Neugebauer, G., 1996, *AJ*, 111, 1025
 Murphy, T.W., Soifer, B.T., Matthews, K., Armus, L., 2001, *ApJ*, 559, 201
 Rigopoulou, D., Spoon, H.W.W., Genzel, R., Lutz, D., Moorwood, A.F.M., Tran, Q.D., 1999, *AJ*, 118, 2625
 Rotundi, A., Brucato, J.R., Colangeli, L., Ferrini, G., Mennella, V., Palombo, E., Palumbo, P., 2002, *Meteoritics*, 37, 1623
 Sargent et al., 2005, in preparation
 Sloan et al. 2005, in preparation
 Spoon, H.W.W., et al., 2004, *ApJS*, 154, 184
 Spoon, H.W.W., et al., 2005, in preparation
 Sylvester, R.J., Kemper, F., Barlow, M.J., de Jong, T., Waters, L.B.F.M., Tielens, A.G.G.M., Omont, A., 1999, *A&A*, 352, 587
 Tielens, A.G.G.M., Allamandola, L.J., 1987, in *Interstellar Processes*, ed. D.J. Hollenbach, H.A. Thronson (Dordrecht: Reidel), 397
 Tielens, A.G.G.M., Meixner, M.M., van der Werf, P.P., Bregman, J., Tauber, J.A., Stutzki, J., Rank, D., 2003, *Science*, 262, 86
 Tran, Q. D., Lutz, D., Genzel, R., et al., 2001, *ApJ*, 552, 527
 van Boekel, R., et al., 2004, *Nature*, 432, 479
 Voors, R.H.M., Waters, L.B.F.M., Morris, P.W., Trams, N.R., de Koter, A., Bouwman, J., 1999, *A&A*, 341, L67
 Voors, R.H.M., Waters, L.B.F.M., de Koter, A., Bouwman, J., Morris, P.W., Barlow, M.J., Sylvester, R.J., Trams, N.R., Lamers, H.J.G.L.M., 2000, *A&A*, 356, 501
 Webber, W.R., 1993, *ApJ*, 402, 188
 Werner, M.W., et al., 2004, *ApJS*, 154, 1
 Wooden, D. H., et al., 1993, *ApJS*, 88, 477